Consequences of composition on morphological and mechanical properties in fully renewable poly(lactide)-poly(farnesene) block copolymers

Milan Den Haese[1,2], Sander Driesen[1,2], Geert Jan Graulus[2], Louis M. Pitet[1*]

[1]*Advanced Functional Polymers Laboratory, Institute for Materials Research (imo-imomec), Hasselt University, Martelarenlaan 42, 3500 Hasselt, Belgium.*
[2] *Biomolecule Design Group, Institute for Materials Research (imo-imomec), Hasselt University, Agoralaan Building D, 3590 Diepenbeek, Belgium.*

Keywords: *Sustainable polymers; renewable thermoplastic elastomers; self-assembling block polymers; flow polymerization; poly(farnesene); poly(lactide)*

ABSTRACT

Reliance on non-renewable fossil resources, sluggish degradability, and limited recycling opportunities encourage the implementation of more sustainable materials and manufacturing practices in society. Poly(lactide) (PLA), an FDA-approved biobased polymer with biodegradable properties has long been studied as a promising alternative. However, there is a need to overcome the inherent brittleness associated with PLA, thereby drastically improving its applicability. We explored the incorporation of hydroxyl-telechelic poly(β-farnesene) (PF) - a biobased, hydrophobic polymer derived from terpenes - as a soft midblock in a PLA-PF-PLA triblock system. The effect of molecular weight and weight fraction of PLA on morphology was studied using SAXS and TEM. Lower molecular weight polymers assembled into a lamellar morphology at high PLA weight fractions, while high molecular weight polymers adopted hexagonally-packed cylinder morphology, and exhibited relatively elastomeric behavior. Tensile studies revealed that mechanical properties can be tuned by altering the PLA composition, with higher weight fractions increasing tensile modulus to 22.1 MPa. Additionally, a comprehensive E-

factor analysis was performed on the block copolymer synthesis in order to highlight the importance of process optimization when designing complex sustainable polymers.

INTRODUCTION

Plastics are found in nearly every consumer product today, from packaging materials and electronic devices to clothing, due to their straightforward production, ease of processing and exceptional durability.[1-4] However, nearly all plastics are derived from non-renewable fossil sources, are only degradable over vast timescales, and are prohibitively difficult to recycle. We are now in the midst of a plastic pollution crisis and are continuing to deplete precious resources.[1, 3, 5] Making substitutions to our commodity polymer platforms with renewable (and/or recyclable) alternatives remains a challenge, predominantly because property matching is difficult.

Exploring renewable, biobased alternatives for plastic materials remains one of the critical strategies in transitioning to a circular economy.[4-10] Extensive efforts have been made to introduce poly(lactide) (PLA), a bio-based polymer, into everyday plastic products.[11-14] PLA is typically made by ring-opening transesterification polymerization (ROTEP) of lactide, which itself is obtained through the anaerobic fermentation of carbohydrates.[15, 16] Additionally, the FDA has approved PLA for food packaging and medical materials such as sutures.[16] Lastly, PLA is a polyester, and can therefore biodegrade under composting conditions without any residual microplastics, tackling a growing concern in the field of environmental health sciences.[16-18]

However, PLA homopolymer is notoriously brittle.[15, 19] Expanding the range of applications for which PLA is suitable can be achieved with block polymers, where the relatively rigid PLA typically acts as a hard block.[20-26] Combining PLA with a softer segment (i.e., poly(butadiene), poly(isoprene)), typically leads to improved elasticity and impact resistance.[27-30] This in turn modifies the overall polymer behavior to exhibit a wide range of properties depending on the respective block compositions.[31-35] Fully renewable PLA-based block polymers with properties targeting elastomeric behavior have been reported, typically utilizing structurally related aliphatic

polyester soft-blocks.[36-40] However, the number of suitable biobased soft-blocks that are amenable to chain extension with PLA remains relatively limited.[41]

One potentially appealing candidate is poly(β-farnesene), a biobased, hydrophobic polymer derived from terpenes, which in turn are a class of natural molecular biomass produced by various plants and animals. They are also a major component of tree resin, an exudate typically obtained from pine trees and conifers.[42] Terpene derivatives such as isoprene, myrcene and farnesene have garnered attention in the field of elastomers thanks to their relatively facile polymerization and tuneability, in addition to being renewable alternatives to commercial petrochemical based diene counterparts. [43-46]

In this study, PLA was incorporated into symmetric ABA triblock copolymers by applying hydroxyl-telechelic poly(β-farnesene) as a macroinitiator for the ROTEP of lactide with the aim of accessing elastomeric materials. To investigate the relationship between the overall molar mass and respective PLA weight compositions, morphological-, thermal-, and mechanical properties were systematically evaluated for the first time. Establishing the connection between mechanical properties and molecular attributes in these fully renewable copolymers highlights some of the opportunities for various applications and challenges that remain for expanded utility.

RESULTS AND DISCUSSION

This work leverages the insights from our previous publication, in which poly(farnesene)- and poly(lactide)-based triblock copolymers were prepared using an unconventional plug flow reactor.[44] We previously showed an efficient synthetic route to prepare differently composed triblocks to augment their mechanical attributes for a broader spectrum of applications. Previously, we reported the synthesis of symmetric ABA-type triblock copolymers using two different samples of poly(farnesene)-diol macroinitiators (4 kg/mol and 30 kg/mol). However, as the focus was primarily on the implementation of various reaction parameters for block copolymer

synthesis using a novel flow reactor, a thorough morphological- and mechanical analysis was not in scope. In this study we prepared a new series of copolymers with various chain-lengths and compositions (i.e., A:B ratios). A series of samples was prepared covering a composition range for poly(lactide) of 20 wt %, 30 wt %, 50 wt %, 70 wt %, and 80 wt %, using the two poly(farnesene)-diol macroinitiators. The resulting block copolymers are hereafter referred to as L_x-F_y-L_x, where x and y reflect the molar mass of PLA and poly(farnesene) (in kg/mol), respectively. Subsequently, the molecular and physical properties of these samples were interrogated with respect to their composition and molar mass. Solution polymerization was selected over bulk polymerization to ensure sufficiently low viscosity for continuous flow operation. While the planar flow reactor is capable of handling viscous systems, the introduction of solid reagents such as lactide presents practical challenges. In terms of sustainability, flow polymerizations offer some appealing features, assuming that the solvent employed can be efficiently recovered (vide infra, E-factor analysis). In batch, solution polymerization additionally provided enhanced mixing, thereby allowing more precise control over molecular weight and block architecture. For the monomer choice, DL-lactide was employed instead of L-lactide. Polymerization of DL-lactide yields amorphous PLA segments, which not only facilitates processing (e.g., melt-pressing at lower temperatures) compared to isomerically pure systems prone to crystallization, but also allows the morphological features to be assessed that result from the mixing thermodynamics rather than induced by crystallization.

PLA composition and molar mass distribution:

Compositions of the block polymers were determined with ^{1}H nuclear magnetic resonance (NMR) spectroscopy (Figure 1). The relative content of PLA repeating units was calculated as the ratio of methine protons in PLA to aliphatic repeating units in the poly(farnesene) side branches (Figure S2). Additionally, size exclusion chromatography (SEC) was used to determine the molar mass, dispersity, and composition of the polymers (Figure 2; Table 1). A quadruplet signal is present at

δ 4.4 ppm for every sample, with the intensity increasing for higher PLA compositions. This peak corresponds to the PLA end groups and increases with intensity as the number of PLA chains increases, presumably arising primarily from transesterification. Increased transesterification is consistent with the increase in dispersity for higher PLA compositions in high molecular weight samples. Additionally, a distinct peak between δ 3.6 – 3.8 ppm can be seen in the higher molecular weight samples as PLA composition increases. This peak is assigned to methyl-ester chain ends that arise from limited methanolysis that occurs during precipitation.

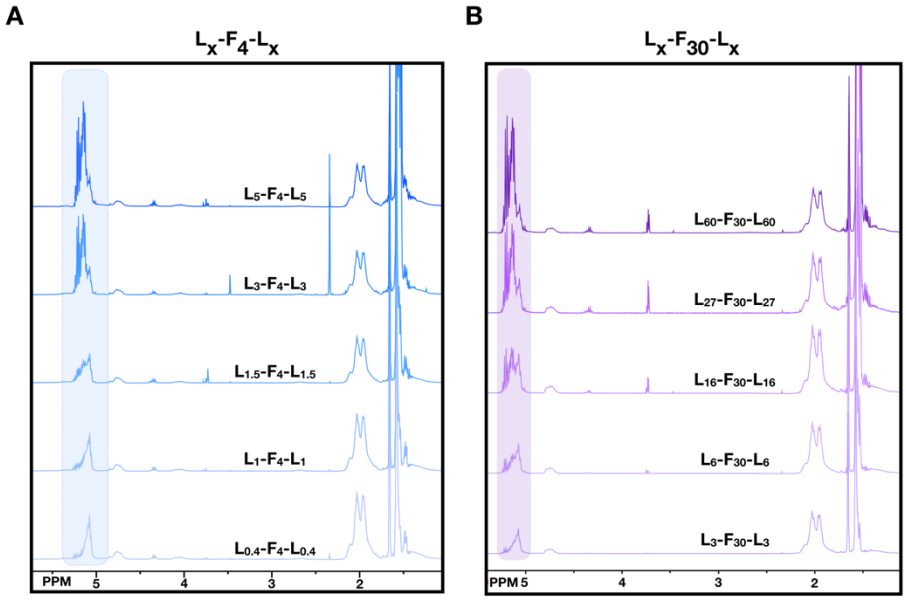

Figure 1. ^{1}H NMR spectra of (A) the shorter and (B) the longer analogs of LFL block copolymers.

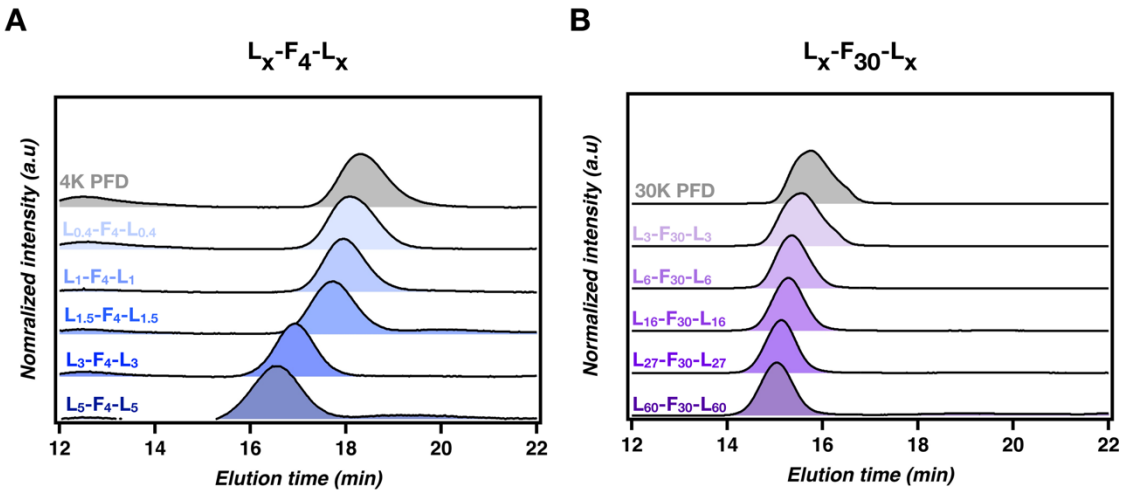

Figure 2. SEC chromatograms for (A) lower and (B) higher molar mass LFL block copolymer series.

Table 1. Summary of ^{1}H NMR and SEC analysis on low- and high molecular weight block copolymer samples.

	Sample name	Target φ_L	M_w (kg/mol) (SEC)[a]	M_n (kg/mol) (SEC)[a]	φ_L (^{1}H NMR)[b]	φ_L (SEC)[c]	Đ[a]
PFD (4 Kg/mol)	$L_{0.4}$-F_4-$L_{0.4}$	0.2	5.1	4.9	0.22	0.16	1.17
	L_1 -F_4-L_1	0.3	6.6	6.3	0.31	0.35	1.17
	$L_{1.5}$-F_4-$L_{1.5}$	0.5	7.2	7.0	0.52	0.41	1.30
	L_3-F_4-L_3	0.7	10.2	10.1	0.64	0.58	1.16
	L_5-F_4-L_5	0.8	13.6	13.6	0.76	0.69	1.17
PFD (30 Kg/mol)	L_3-F_{30}-L_3	0.2	43.1	43.1	0.19	0.21	1.15
	L_6-F_{30}-L_6	0.3	47.7	47.7	0.34	0.28	1.39
	L_{16}-F_{30}-L_{16}	0.5	67.5	67.4	0.52	0.49	2.28
	L_{27}-F_{30}-L_{27}	0.7	90.4	89.4	0.73	0.62	3.39
	L_{60}-F_{30}-L_{60}	0.8	158.2	158	0.81	0.78	1.27

[a] Determined from SEC in chloroform from multi-angle laser light scattering detector, with dn/dc calculated internally based on sample concentration and assuming 100% mass elution. [b] wt % composition of L-block determined from relative integration of ^{1}H NMR spectroscopy [c] wt % composition as determined indirectly from the molar mass from SEC.

Experimentally determined compositions closely matched the theoretical targets for both the high molar mass and low molar mass sample sets (Table 1). The minor deviations in PLA compositions between SEC and ^{1}H NMR analyses can be attributed to lower molecular weight polymer chains

resulting from transesterification. These small signals presumed to be from homopolymer were not integrated during the SEC analysis, yet still contribute to ^{1}H NMR signals. We therefore expect the PLA contribution in ^{1}H NMR analysis to be slightly higher, especially in higher PLA weight contribution samples.

The low dispersities observed for all samples are indicative of a controlled polymerization process. Furthermore, SEC analyses indicated a subtle deviation from the target PLA composition at higher PLA contributions (this is especially evident in L_3-F_4-L_3, L_5-F_4-L_5 and L_{27}-F_{30}-L_{27}). Higher PLA content corresponds with higher molecular weight, which can influence the conversion rate. Specifically, the growth in chain lengths of the polymer can impede diffusion toward reactive chain end-groups and reduce the mobility of lactide monomers which also decrease in concentration, slowing the reaction kinetics. In addition to the factors mentioned, it's important to consider that ROTEP is typically a reversible (i.e., equilibrium) process. Higher molecular weight polymers tend to shift the equilibrium toward polymerization products, thus potentially decelerating the overall reaction rate and result in smaller block copolymer fragments that are omitted in the SEC analysis. [47, 48]

Analysis of thermal properties:

All polymer samples were analyzed via differential scanning calorimetry (DSC) to investigate their thermal properties and correlate them to molecular characteristics. The glass transition (T_g) of PLA consistently increases with increasing molar mass in the shorter homologues, consistent with expectations (Figure 3a; Figure S4).[49] The distinct T_g observed for the individual blocks suggests a relatively strong immiscibility between the two blocks, which is consistent with previous reports on PLA block polymers having a relatively hydrophobic, hydrocarbon based block.[29, 50, 51] The notable exception to this is sample $L_{0.4}$-F_4-$L_{0.4}$, which is not entirely surprising based on the very short PLA segments. This shortest block polymer has only 3 repeating units of PLA per segment

on average. Such short blocks are likely nearly miscible with the hydrophobic PFD blocks, which is consistent with the X-ray analysis (*vide infra*).

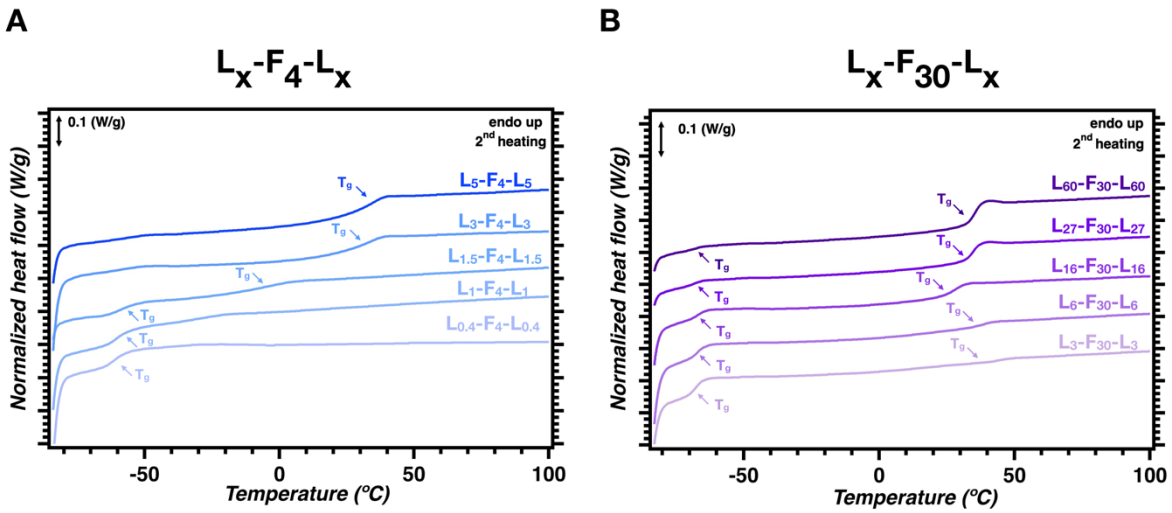

Figure 3. DSC thermograms of LFL block copolymers for (A) lower and (B) higher molar mass homologues.

Morphological behavior

The meso-scale morphological characteristics and domain spacing were determined at various temperatures (20–140 °C) using small-angle X-ray scattering (SAXS). The results indicate a clear interplay between PLA composition, poly(farnesene) molecular weight, and temperature in relation to microphase organization. In the case of the shorter chain sample set (L_x-F_4-L_x), phase-separated structures were observed, albeit lacking long-range order. This was the case for compositions of φ_L lower than 70 wt % due to the small number of PLA repeating units per segment. On the other hand, higher PLA compositions (L_3-F_4-L_3 and L_5-F_4-L_5) exhibit patterns consistent with lamellar organization, as evidenced by sharp signals at q* and 2q. The position of the principle scattering vectors q* correspond with domain spacings (d*) of 11.7 nm and 13.7 nm for L_3-F_4-L_4 and L_5-F_4-L_5, respectively (Figure 4 A,B). These peaks correspond to the 100 and 200 planes of alternating lamellae.[52-54] Conversely, in the case of higher molecular weight samples L_x-

F_{30}-L_x, the samples L_3-F_{30}-L_3 and L_6-F_{30}-L_6 exhibit pronounced peaks at q* and √3q, corresponding to principal domain spacings of 17.5 nm and 21.6 nm, respectively (Figure 5 A,B). These patterns are characteristic of hexagonally packed PLA cylinders in a poly(farnesene) matrix.[52, 55]

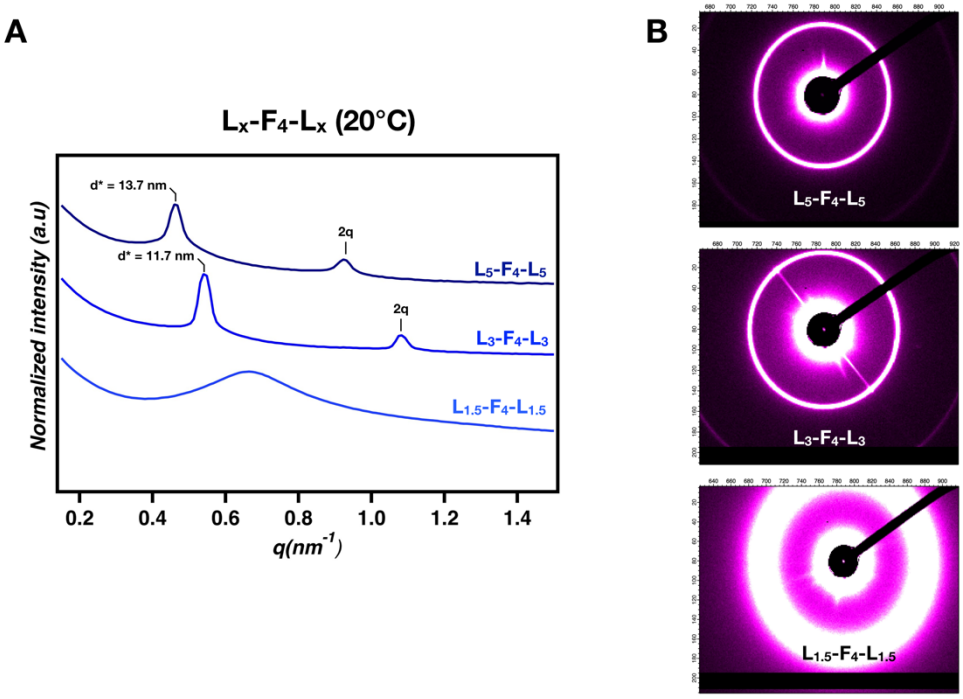

Figure 4: SAXS summary of low molecular weight LFL block copolymers at 20°C (A), including the corresponding 2D patterns used for azimuthal integration (B).

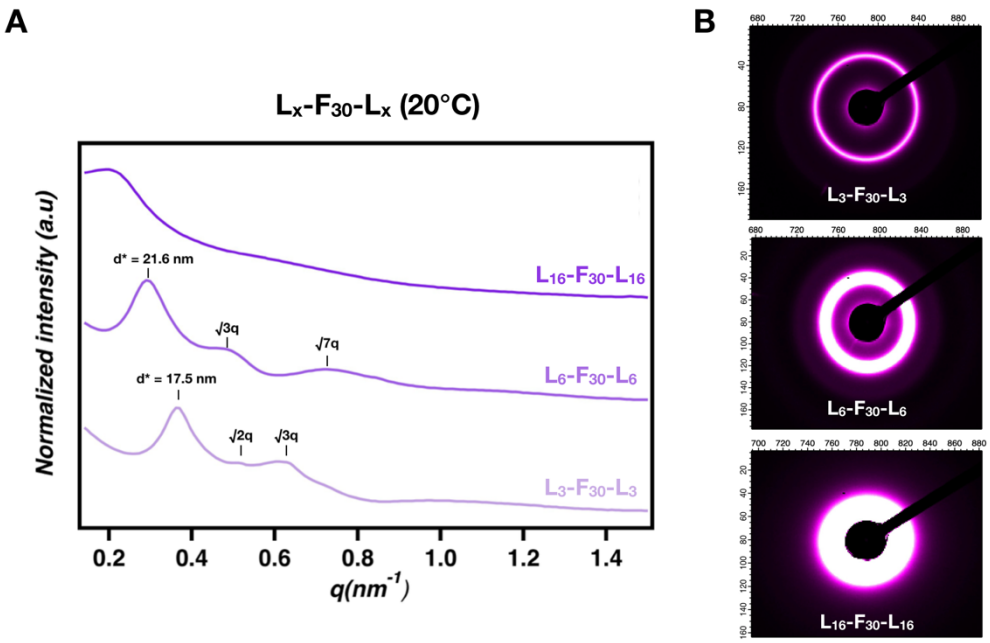

Figure 5**:** SAXS summary of high molecular weight LFL block copolymers at 20 °C (A), including the corresponding 2D patterns used for azimuthal integration (B).

The self-assembly of block copolymers is governed by thermodynamic considerations, including the Flory-Huggins interaction parameter (χ), which quantifies in an empirical manner the free energy cost per monomer in a situation when two unlike units want to segregate and can be estimated by models such as Random Phase Approximation (RPA) or self-consistent field theory (SCFT).[31, 56, 57] The immiscibility of the different polymer segments is the essence of the driving forces for microphase segregation.[58] The combination of relative composition and molar mass essentially determines the morphology that emerges, such as lamellar and [hexagonally packed] cylindrical structures, as well as the size of the domains and their spacing.[58] For low molecular weight LFL, microphase separation occurs only at high PLA compositions (> 50 wt %) as lower compositions have only a few repeating units of PLA on each side of the PF block, and thus mixing (i.e., disorder) is favored.[59] Higher PLA compositions (L_3-F_4-L_3 and L_5-F_4-L_5), however, show scattering peaks (q, 2q) that are indicative of a lamellar morphology. The relatively flat interfaces associated with lamellae are adopted despite the strong asymmetry in the composition of these

samples. This is most likely related to two mutually reinforcing effects: the conformational asymmetry typical of PLA-containing blocks[60, 61], and the short-chain branching of the PFD midblock.[62] The observation of compositionally asymmetric lamellae in block copolymers with branched architectures in one of the blocks is in line with both SCFT models and experimental results. Briefly, the boundaries between morphologies in the phase diagram are predicted to shift substantially compared with classical diblock copolymers.[63, 64] For example, lamellae are predicted to form in a block polymer that is rich in the linear component (i.e., PLA). Highly asymmetric lamellae were observed experimentally in branched PLA-based block polymers in the past.[65, 66] In contrast, volumetric asymmetry in high molecular weight LFL samples results in microphase separation in lower PLA weight fractions (i.e., $\phi_L < 50$). Larger PF blocks relax by curving the interface towards shorter PLA blocks, forming hexagonally packed cylinders of PLA in a matrix of PF. [60, 67-71]

Individual LFL block copolymer samples were also analyzed by SAXS at various temperatures, heating the sample from 20 °C to 120 °C. For lower molecular weight polymers that exhibit microphase separation (L_3-F_4-L_3 and L_5-F_4-L_5), significant broadening of the peaks occurred at 80 °C for both samples, attributed to increased interphase diffusion, and less definition in the interface between the microdomains. At 120 °C, neither sample displays long range organization. This can also be seen on the 2D SAXS images where the concentric rings become broadened at higher temperatures (Figure 6 A,C). Upon cooling, both samples regain the organized morphologies. Additionally, the increased rigidity of the polymer chains fixes the microphase conformations as they become more constrained. As a result, the peaks corresponding to the lamellar micro-domains become narrower and the 2D SAXS image becomes slightly more intense (Figure 6 B,D). The effect of heating and consequent cooling is the same for higher molecular weight samples with low PLA compositions (L_3-F_{30}-L_3 and L_6-F_{30}-L_6), although the peak broadening is less pronounced, even at 140 °C, suggesting that the increased molecular weight of the sample significantly retards molecular diffusion (Figure 7). Remarkably, in the high

molecular weight L_3-F_{30}-L_3 sample, a small but prominent peak at √2q is consistent with body-centered cubic spheres (BCC spheres) with a domain spacing of 12.5 nm.[72] This is most likely due to annealing, whereby extended periods at high temperatures can promote metastable phases that do not appear when heating the sample.[73, 74]

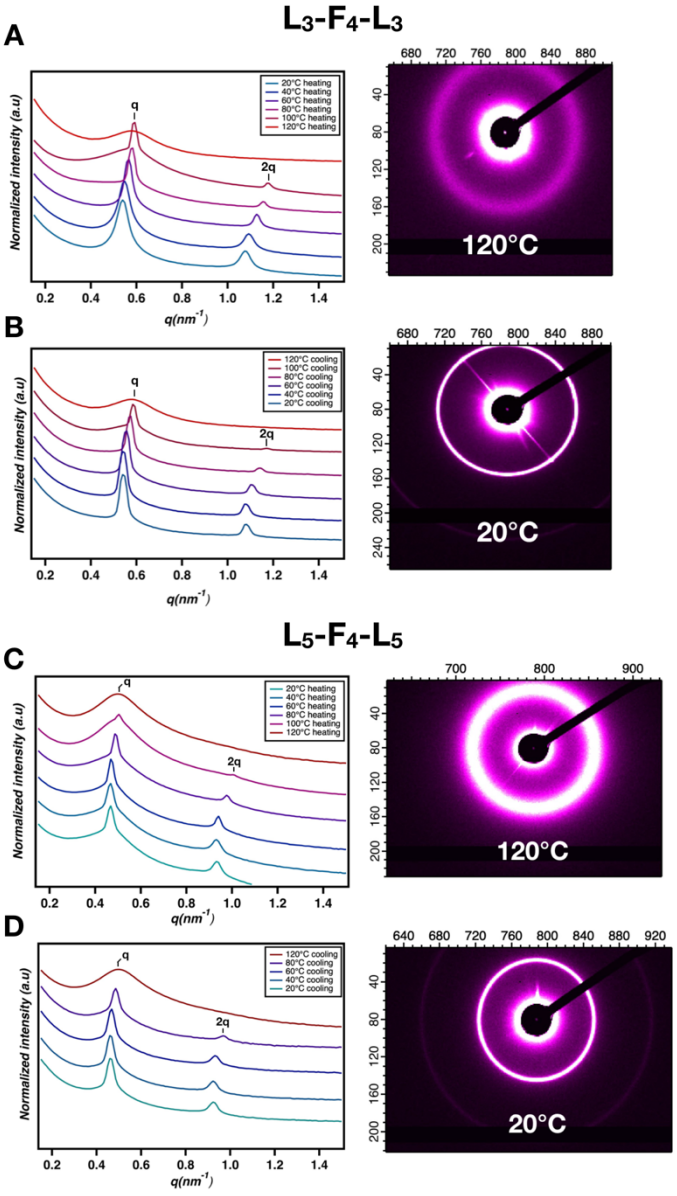

Figure 6: Summary of simultaneous heating- / cooling cycles and SAXS analysis for low molecular weight LFL block copolymers. (A,B) 1D and 2D SAXS graph for heating and cooling of

L_3-F_4-L_3, respectively. (C,D) 1D and 2D SAXS graph for heating and cooling of L_5-F_4-L_5, respectively.

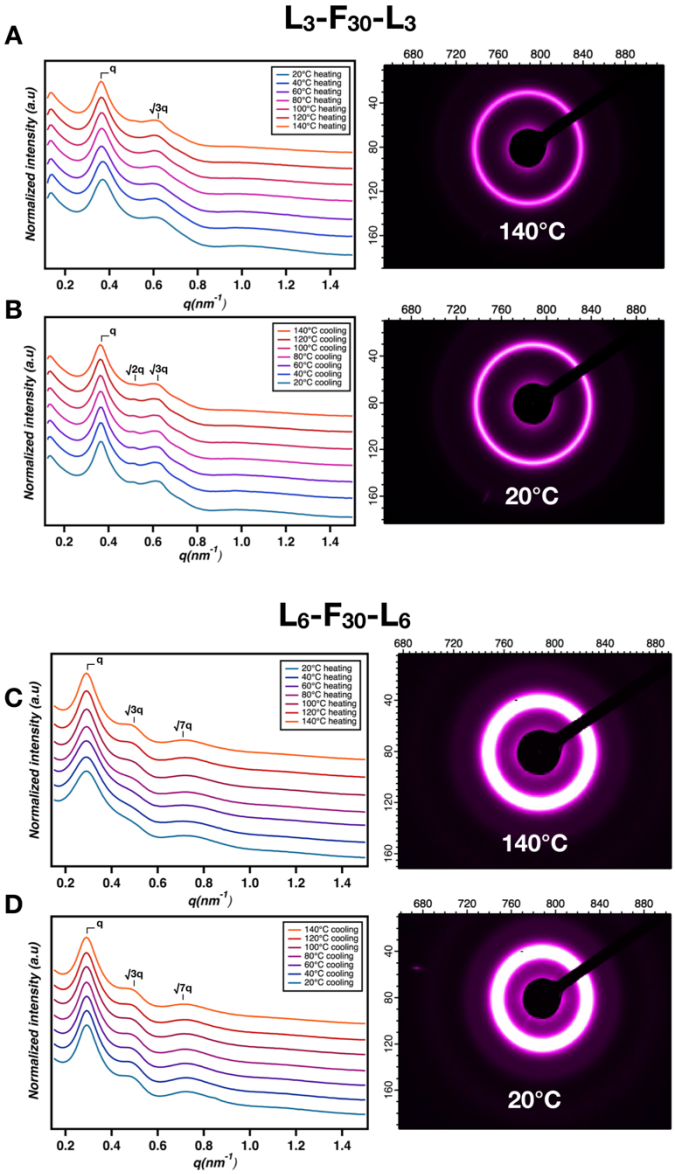

***Figure 7*: Summary of simultaneous heating- / cooling cycles and SAXS analysis for high molecular weight LFL block copolymers. (A,B) 1D and 2D SAXS graph for heating and cooling of L_3-F_{30}-L_3, respectively. (C,D) 1D and 2D SAXS graph for heating and cooling of L_6-F_{30}-L_6, respectively.**

Transmission electron microscopy (TEM):

All samples that showed microphase separation based on the SAXS analysis were visually analyzed using transmission electron microscopy (TEM). For the low molecular weight sample series, worm-like structures were observed for L_3-F_4-L_3 and L_5-F_4-L_5, consistent with the lamellar microphase organization displayed in the SAXS profiles (Figure 8 A,B). For L_5-F_4-L_5, it was clear that the lamellar organization was more pronounced, with the average lamellar thickness increasing from 6.2 nm for L_3-F_4-L_3 to 10.6 nm for L_5-F_4-L_5. The increase in lamellar thickness agrees with the SAXS data. However, the domain sizes differ slightly yet fall within the same range. Additionally, the TEM analysis suggests the absence of long-range order, as the lamellar worm-like structures are randomly oriented in the L_5-F_4-L_5 samples and very localized in L_3-F_4-L_3. Nevertheless, average dimensions measured from micrographs are consistent with the SAXS measurements and corroborate the morphology. Likewise, samples L_3-F_{30}-L_3 and L_6-F_{30}-L_6 showed microphase separation that supported the respective SAXS data (Figure 8 C,D). Localized hexagonally packed circular patterns were present in both samples which were lighter in color than the surrounding matrix, indicating that the circles were composed out of PLA. For L_3-F_{30}-L_3, the average center-to-center distance between cylinders was 24.5 nm with an average cylinder diameter of 11.7 nm. These dimensions increased in size with increasing PLA content (L_6-F_{30}-L_6), with the average center-to-center distance between cylinders being 34.5 nm with an average diameter of 22.3 nm. Although the images suggest that the block copolymer is microphase separated, the lack of long-range order suggested by SAXS profiles is corroborated by the TEM images.

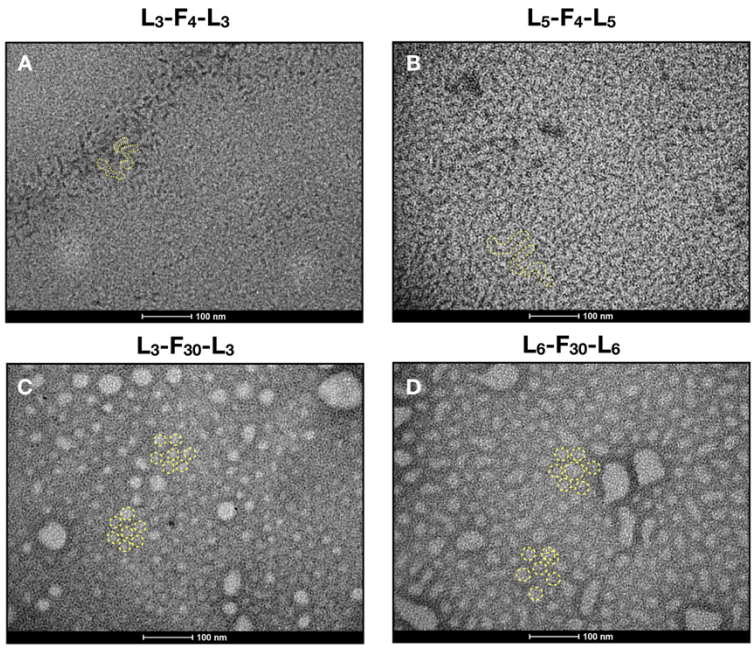

Figure 8: TEM analysis of LFL block copolymers at 135Kx zoom. (A,B) low molecular weight LFL displaying localized lamellar microphase separation. (C,D) high molecular weight LFL displaying hexagonally packed cylinders.

Table 2: Summary of dimensional analysis performed on the TEM images of different LFL block copolymer samples.

PFD molar mass (kg/mol)	PLA composition (wt %)	Inter-cylinder space (nm)	Cylinder diameter (nm)	Lamellar thickness (nm)
4	70	/	/	6.2 ± 1.1
4	80	/	/	10.6 ± 2.0
30	20	24.7 ± 2.6	11.7 ± 1.7	/
30	30	34.5 ± 4.4	22.3 ± 2.6	/

Notably, mesoscale phase separation was also observed in higher PLA compositions for high molecular weight poly(farnesene), albeit lacking any long-range order. It is difficult to conclude any organized morphology, probably owing to the higher level of entanglements, large incompatibility between PLA and PFD blocks, and lack of annealing employed (Figure S5).

Nevertheless, the dimensions are significantly larger, commensurate with the higher molar masses.

Mechanical analysis of high molecular weight LFL block polymers

Selected L_x-F_{30}-L_x samples were subjected to tensile testing experiments, whereby the melt compressed molded samples were cut into dog-bone shapes (35 mm × 2 mm × 1 mm) and mechanically extended until they broke. L_3-F_{30}-L_3 exhibited a low modulus (92.3 kPa) and broke at relatively high strain (98%). L_6-F_{30}-L_6 has a higher modulus in addition to a reduced strain. Lastly, when the PLA content is increased to 50 wt %, stiffness is further increased, and the strain at break is reduced to 38%. The increasing brittleness is coupled with a drastic decrease in flexibility as the Young's modulus increases to 411.4 kPa (Figure 9). Samples with very high PLA content, L_{27}-F_{30}-L_{27} and L_{60}-F_{30}-L_{60}, far exceeded the Young's modulus of lower composition samples (13.5 MPa and 22.1 MPa, respectively) but compromise in their elastomeric behavior owing to the low strain at break. As the poly(farnesene) component diminishes, the overall mechanical properties will more closely resemble those of high molecular weight PLA homopolymer (i.e., a very tough, but brittle material).[25, 27, 30] The very low volume fractions of soft-block material in L_{27}-F_{30}-L_{27} and L_{60}-F_{30}-L_{60} allow for very subtle flexibility before breaking at minimal deformation. Referring to literature, numerous PLA based block copolymers designs have been investigated for their mechanical properties. Comparing the data for a selection of materials highlighted in a recent perspective study, it becomes clear that our PLA-based copolymer design showcases modest mechanical properties.[25] We postulate this behavior to originate from several molecular features. Firstly, as mentioned, we used racemic DL-lactide instead of isomerically pure L-lactide as a monomer and assumed that the amorphous nature of the resulting PLA chain would enhance elasticity without compromising toughness. However, the lack of crystallinity leads generally to weak and brittle materials. The lack of mechanical integrity is likely exacerbated, as

steric repulsion from sidechains on the PF midblock may inhibit chain entanglement and therefore reduce resistance to fracture.

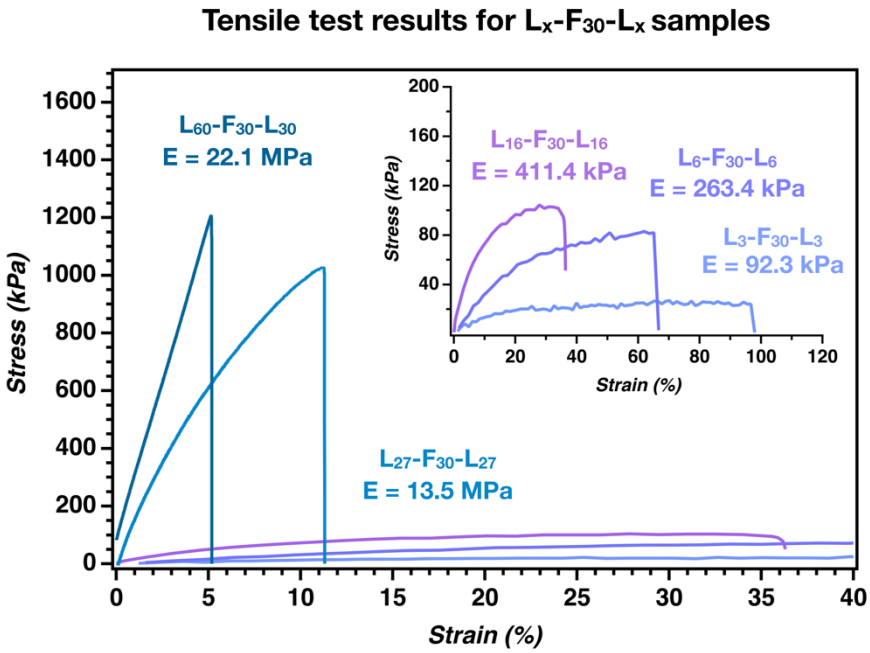

Figure 9: Stress/strain curves for high molecular weight LFL block copolymers

Additionally, cyclic tensile tests were performed on the L_x-F_{30}-L_x polymers with 20%, 30%, and 50% PLA compositions in order to test the durability of the mechanical properties. All samples were elongated to 20% strain at 100 mm per minute. The recorded stress in kPa after each cycle provided insight into the decrease of the Young's modulus for each sample. Lower PLA compositions (L_3-F_{30}-L_3) exhibit very elastic behavior owing to the higher contribution of the soft block component, with the hard PLA segment providing minimal integrity, yet enough to allow for elastic characteristics, as well as a minimal loss of mechanical properties over repeated stretching. This contrasts with increased PLA compositions (L_6-F_{30}-L_6 and L_{16}-F_{30}-L_{16}) where a significant loss in the Young's modulus is observed after the first elongation to 20% strain (Figure 10). Increased PLA compositions reduce the flexibility of the polymers and therefore its resistance to permanent deformation. Finetuning of the PLA composition will enable a wide array of

mechanical properties with ranging degrees of elasticity. However, to accommodate a wide array of applications, elastomers need to exhibit various degrees of toughness as some uses exert high forces on the materials, for example windshields wipers, snowmobile tracks, etc. One way to improve the overall toughness of the polymer samples described in this study would be to increase the molecular weight of the poly(farnesene) midblock beyond 30 kg/mol. Another option would be to functionalize side chains of the poly(farnesene)-diol via consecutive epoxidation and hydrolysis, to yield hydroxyl groups along the backbone that can be used to initiate ROP of lactide. The resulting bottlebrush polymers would provide additional mechanisms of tunability, as grafting density and weight compositions can be modulated with respect to each other.[28] For the present systems, however, it is worth noting that their distinct high T_g–low T_g–high T_g architecture may enable alternative functionalities beyond bulk mechanical reinforcement. In particular, this architecture could promote adhesive behavior, as the combination of soft, low-T_g domains with rigid, high-T_g end blocks is known to induce tack.[75] We therefore propose that future studies assess the adhesive properties of these materials, which may open pathways toward their use in pressure-sensitive adhesives or related soft-matter applications. Additionally, the block copolymers described here may be suitable as compatibilizers for existing-, or novel polymer blends in an effort to improve mechanical properties.

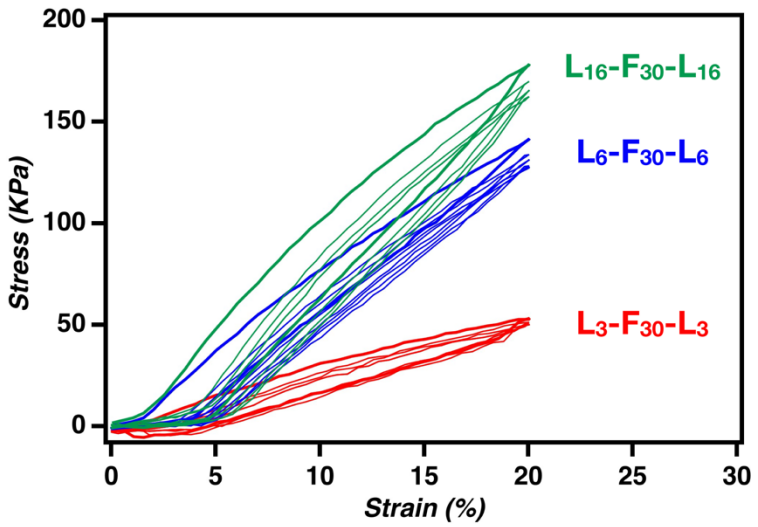

Figure 10: Cyclic stress strain curves for high molecular weight LFL block copolymers

Quantifying waste generation in LFL block copolymer synthesis: an E factor perspective.

With the ever-growing demand for society to transition to circular economies, renewables and bio-based resources play an important role. Waste generation in chemical manufacturing is among the biggest contributers to adverse environmental effects. This led to a paradigm shift in how the efficiency of chemical processes is assessed.[76] The E (environmental) factor, introduced by Roger Sheldon in the 1990s, brought attention to the amount of non-product material, such as solvents, by-products and reagents, that is generated using the formula:

$$E\ factor = \frac{weight\ of\ raw\ materials - weight\ of\ desired\ product}{weight\ of\ desired\ product}$$

In doing so, value is given to the waste of a chemical process as opposed to the more traditional *atom economy* metric, whereby efficiency is determined based only on the molecular weights of the initial reagents and products. A lower E-factor suggests a lower environmental impact, and years of its implementation in the chemical industry has given valuable insight as to how the E-factor compares for various processes (Table 3).

Table 3: A summary of E-factors within the chemical industry. Adapted from R. A. Sheldon, *Green Chemistry*, 2023, 25, 1704-1728

Industry	Product tonnage (p/a)	E-factor (kgs/kg product)
Oil refining	10^6-10^8	<0.1
Bulk chemicals	10^4-10^6	<1-5
Fine chemicals	10^2-10^4	5-50
Pharmaceuticals	10-10^3	25-100

Using the above formula, an E-factor was calculated for LFL block copolymers and compared to the synthesis of PLA homopolymer using an analogous synthesis method (i.e. in batch). Assuming 90% yield and 90% solvent recovery, E-factor ranged between 0.26 and 0.67, depending most critically on the weight composition of PLA in the final construct. The biggest determining factor is the concentration of lactide monomer (relative to solvent) in the initial reagent mixture, with higher concentrations resulting in less solvent loss per kg of product formed. For the same reason, higher PLA weight compositions require more solvent per kg product due to the increased lactide monomer. When compared to the synthesis of PLA homopolymer, block copolymer synthesis is more efficient per kg product formed, largely because solvent is substituted with a component that ultimately is incorporated into the final product. (Table S2), (Figure 11).

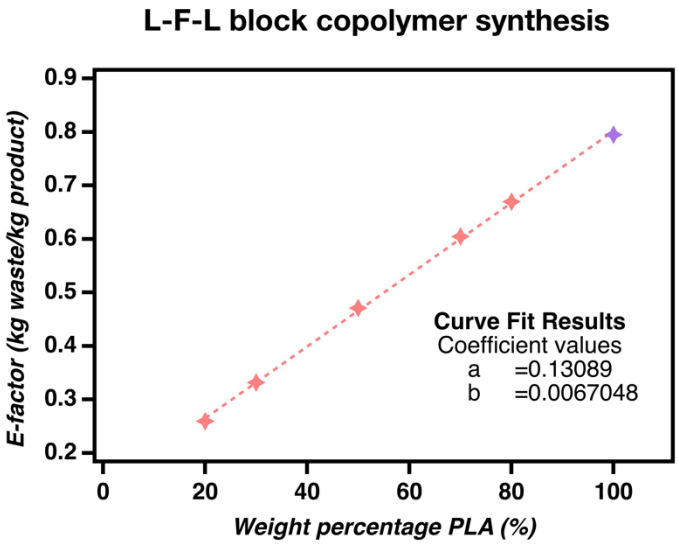

Figure 11: Effect of increasing the PLA weight percentage on the E-factor in LFL block copolymer synthesis. For reference, the synthesis of PLA homopolymer is indicated in purple on the graph.

The polynomial fit used to quantify the effect of PLA molecular weight in homopolymer synthesis suggests that from low to moderate degrees of polymerization (50 – 150), the E-factor decreases as product mass increases faster than waste generation. The quadratic term eventually catches up, with the E-factor plateauing as reaction efficiency starts to diminish. Additionally, extrapolation of the data gives us the most efficient degree of polymerization by taking the derivative:

$$\frac{dE}{dDP} = -0.00016558 + 2 * 3.3306 * 10^{-7} * DP$$

and setting it to zero:

$$0 = -0.00016558 + 6.6612 * 10^{-7} * DP$$

To solve for DP:

$$DP = \frac{0.00016558}{(6.6612 * 10^{-7})} = 248.6$$

Using these data extrapolations, experimental set-ups can be modulated to optimize efficiency.

Comparing the effect of weight fraction PLA incorporated in the LFL block copolymers provides additional insight into the ROTEP of lactide. As shown in Figure 11, increasing the PLA weight fraction results in a linearly increasing E-factor, described by the equation:

$$E(x) = 0.12604 + 0.0068271 * x$$

where x represents the PLA weight percentage, and E(x) is the corresponding E-factor. This linear relationship indicates that for every 1% increase in PLA content, the E-factor increases by approximately 0.00683 units. Assuming a final product mass of 1 gram, this corresponds to an increase in waste of roughly 6.83 mg per 1% increase in PLA. This emphasizes how process design decisions—such as maintaining a constant lactide concentration across samples—can significantly affect green metrics. It demonstrates that ROTEP of lactide does not become necessarily less sustainable as weight fractions are increased, it's that the conditions needed to scale its contribution in the block copolymer increase the amount of starting materials (i.e. solvent).

Analyses like the one performed in this study tell us that E-factor metrics are not just chemistry dependent; they are also process dependent and are crucial when optimizing reactions when sustainability and eventual scale-up is the goal. Employing continuous flow production protocols in the preparation of complex block copolymers can offer significant advantages in terms of waste minimization and efficiency.

Importantly, the E-factor calculations employed here neglect the process required to manufacture the poly(farnesene) mid-blocks. However, this process is already conducted on a commercial scale, and most likely has a minimal impact on the total E-factor. It should be noted however, that in terms of biodegradability, the incorporation of farnesene segments alters the degradation pathway. Specifically, the PLA blocks, which contain hydrolytically labile ester bonds, are expected to degrade readily under composting conditions. In contrast, the farnesene domains, being hydrocarbon-based and non-hydrolyzable, are more resistant and will likely degrade more slowly.[77] This reduced ester content, and the increased hydrophobicity introduced by farnesene

411 are likely to lower the overall degradation rate relative to pure PLA. Nevertheless, as farnesene
412 is a bio-based terpene derivative, we anticipate that it will undergo slow oxidative and microbial
413 breakdown over extended timescales.[78] However, the exact biodegradation pathways for the
414 polyfarnesene materials requires a closer evaluation to determine concretely.
415
416 **CONCLUSION**
417 We have synthesized a variety of PL-PF-PL block copolymers with varying PLA weight
418 compositions and PF molecular weight and demonstrated an intricate relationship between the
419 two parameters using numerous analytical techniques. Using ^{1}H-NMR and SEC analysis we
420 verified the incorporation of a target PLA composition with a high degree of precision. These
421 results allude to a change in microphase separation when going from low- to high molecular
422 weight block copolymers, which was confirmed using SAXS analysis and TEM imaging. Low
423 molecular weight block copolymers self-assemble into lamellar microdomains, with the lamellar
424 thickness being proportional to the weight composition of PLA, whereas high molecular weight
425 samples tend to form hexagonally packed cylinders of PLA in a matrix of poly(farnesene), with
426 cylinder diameter and inter-cylinder distances being proportional to the PLA composition.
427 Additionally, we demonstrated that in order to obtain elastomeric properties, the LFL block
428 copolymers should have a high molecular weight (>30 kg/mol) as the periodicity in the cylindrical
429 microdomains efficiently store potential energy, leading to typical elastomer-like mechanical
430 properties at low PLA weight compositions. These mechanical properties were then investigated
431 using a tensile tester, where it was clear that even a small compositional change (L_3-F_{30}-L_3 to L_6-
432 F_{30}-L_6) can have dramatic influence on the elastomeric behavior. Increasing PLA compositions
433 even further (L_{27}-F_{30}-L_{27} and L_{60}-F_{30}-L_{60}) will drastically increase the Young's modulus but
434 significantly compromise flexibility. As for lower molecular weight block copolymers, no real
435 elastomeric effect is present across the spectrum of PLA weight compositions, with low

compositions behaving like a viscous fluid which can potentially be studied for adhesive properties in a follow up study.

Overall, this study provides us with a very clear overview of the mechanical-, thermal-, and morphological changes that occur when changing the molecular weight, and the weight composition of the hard block in a fully renewable ABA block copolymer system. These results provide a basic guideline of what polymer composition to target in order to achieve specific material properties for various applications, in addition to some detailed insight into the molecular mechanisms at play that lead to the broad spectrum of polymer properties. Notably, the highest molar mass samples exhibit material properties that fall far short of other PLA-containing triblock copolymers. We surmise that this may be a function of the molecular architecture of the polyfarnesene block and we are keen to further explore the consequences of conformation on physical attributes for these fully renewable thermoplastics. Finally, a study into the E-factor analysis of LFL block copolymer synthesis compared to PLA homopolymer synthesis prepared using an analogous reaction protocol highlights the effect of experimental conditions in the overall sustainability of various materials, as well as steps that can be taken to minimize the overall E-factor.

ASSOCIATED CONTENT

Supporting Information

The Supporting Information is available free of charge at:

Additional experimental details, materials, and methods, including ^{1}H NMR spectra, GPC chromatograms, DSC thermograms, and TEM micrographs.

AUTHOR INFORMATION

Corresponding Author

Louis M. Pitet. – Advanced Functional Polymers (AFP) Group, Institute for Materials Research (imo-imomec), Hasselt University, Martelarenlaan 42, 3500 Hasselt, Belgium; orcid.org/0000-0002-4733-0707; Email: louis.pitet@uhasselt.be

Authors

Milan Den Haese – Advanced Functional Polymers (AFP) Group, Institute for Materials Research (imo-imomec), Hasselt University, Martelarenlaan 42, 3500 Hasselt, Belgium; https://orcid.org/0000-0003-1932-5932;

Sander Driesen –Biomolecules Design Group (BDG), Institute for Materials Research (imo-imomec), Hasselt University, Martelarenlaan 42, 3500 Hasselt, Belgium; https://orcid.org/0000-0003-1216-9498

Geert-Jan Graulus – Biomolecules Design Group (BDG), Institute for Materials Research (imo-imomec), Hasselt University, Martelarenlaan 42, 3500 Hasselt, Belgium; https://orcid.org/0000-0001-5445-3396

Author Contributions

The manuscript was written through contributions from all authors. All authors have approved the final version of the manuscript.

Funding

The authors are grateful for funding from the Bijzonder Onderzoeks Fonds (BOF) scheme under contract BOF22KP04 and from the Flemish Research Foundation (FWO) under contract G092023N and contract 1S19023N. Additionally we acknowledge the BM26 (DUBBLE) Beamline at the European Synchrotron Radiation Facility (ESRF) for provision of synchrotron radiation facilities under proposal number A26-2-984.

Notes

The authors declare no conflicts.

ACKNOWLEDGMENTS

The authors are grateful for helpful assistance from dr. Martin Rosenthal from the BM26 (DUBBLE) Beamline at the European Synchrotron Radiation Facility (ESRF).

REFERENCES

1. Zhu, Y.; Romain, C.; Williams, C. K., Sustainable polymers from renewable resources. *Nature* **2016,** *540,* 354-362.

2. Kaplan Sarısaltık, A.; Gulden, T.; Boks, C., A visual scoping review of plastic consumption in everyday life. *Clean. Responsible Consum.* **2025,** *16,* 100248.

3. Nayanathara Thathsarani Pilapitiya, P. G. C.; Ratnayake, A. S., The world of plastic waste: A review. *Clean. Mater.* **2024,** *11,* 100220.

4. Huang, S.; Dong, Q.; Che, S.; Li, R.; Tang, K. H. D., Bioplastics and biodegradable plastics: A review of recent advances, feasibility and cleaner production. *Sci. Total Environ.* **2025,** *969,* 178911.

5. Chen, Q.; Auras, R.; Corredig, M.; Kirkensgaard, J. J. K.; Mamakhel, A.; Uysal-Unalan, I., New opportunities for sustainable bioplastic development: Tailorable polymorphic and three-phase crystallization of stereocomplex polylactide by layered double hydroxide. *Int. J. Biol. Macromol.* **2022,** *222,* 1101-1109.

6. Rosenboom, J.-G.; Langer, R.; Traverso, G., Bioplastics for a circular economy. *Nat. Rev. Mater.* **2022,** *7,* 117-137.

7. Jihoon, S.; Kim, Y.-W.; Kim, G.-J., Sustainable Block Copolymer-based Thermoplastic Elastomers. *Appl. Chem. Eng.* **2014,** *25*.

8. Wang, Z.; Yuan, L.; Tang, C., Sustainable Elastomers from Renewable Biomass. *Acc. Chem. Res.* **2017,** *50,* 1762-1773.

9. Schneiderman, D. K.; Hillmyer, M. A., 50th Anniversary Perspective: There Is a Great Future in Sustainable Polymers. *Macromolecules* **2017,** *50,* 3733-3749.

10. Fagnani, D. E.; Tami, J. L.; Copley, G.; Clemons, M. N.; Getzler, Y. D. Y. L.; McNeil, A. J., 100th Anniversary of Macromolecular Science Viewpoint: Redefining Sustainable Polymers. *ACS Macro Lett.* **2021,** *10,* 41-53.

11. Bednarek, M.; Grabowski, M., Polylactide/poly(vinyl monomer) block copolymers for specific applications. *Polym. Rev.* **2024,** *64,* 898-938.

12. Nakajima, H.; Dijkstra, P.; Loos, K., The Recent Developments in Biobased Polymers toward General and Engineering Applications: Polymers that are Upgraded from Biodegradable Polymers, Analogous to Petroleum-Derived Polymers, and Newly Developed. *Polymers* **2017,** *9*,523.

13. Madhavan Nampoothiri, K.; Nair, N. R.; John, R. P., An overview of the recent developments in polylactide (PLA) research. *Bioresour. Technol.* **2010,** *101,* 8493-8501.

14. Höglund, A.; Odelius, K.; Albertsson, A.-C., Crucial Differences in the Hydrolytic Degradation between Industrial Polylactide and Laboratory-Scale Poly(L-lactide). *ACS Appl. Mater. Interfaces* **2012,** *4,* 2788-2793.

15. Ramezani Dana, H.; Ebrahimi, F., Synthesis, properties, and applications of polylactic acid-based polymers. *Polym. Eng. Sci.* **2023,** *63,* 22-43.

16. Swetha, T. A.; Bora, A.; Mohanrasu, K.; Balaji, P.; Raja, R.; Ponnuchamy, K.; Muthusamy, G.; Arun, A., A comprehensive review on polylactic acid (PLA) – Synthesis, processing and application in food packaging. *Int. J. Biol. Macromol.* **2023,** *234,* 123715.

17. Zaaba, N. F.; Jaafar, M., A review on degradation mechanisms of polylactic acid: Hydrolytic, photodegradative, microbial, and enzymatic degradation. *Polym. Eng. Sci.* **2020,** *60,* 2061-2075.

18. Ramírez-Herrera, C.; Flores-Vela, A.; Torres-Huerta, A.; Domínguez-Crespo, M. A.; Palma Ramírez, D., PLA degradation pathway obtained from direct polycondensation of 2-hydroxypropanoic acid using different chain extenders. *J. Mater. Sci.* **2018,** *53*.

19. Musa, L.; Krishna Kumar, N.; Abd Rahim, S. Z.; Mohamad Rasidi, M. S.; Watson Rennie, A. E.; Rahman, R.; Yousefi Kanani, A.; Azmi, A. A., A review on the potential of polylactic acid based thermoplastic elastomer as filament material for fused deposition modelling. *J. Mater. Res. Technol.* **2022,** *20,* 2841-2858.

20. Zhai, Y.; Ghaffar, S.; Zhao, Y.; Zhang, Y.; Kong, L.; Li, J.; Lei, Y.; Jiang, Y., Hydrogen-Bond-Network-Driven Biodegradable PLA Elastomer with High Strength and Toughness. *ACS Appl. Polym. Mater.* **2025,** *7,* 5684-5695.

21. Ding, Y.; Lu, B.; Wang, P.; Wang, G.; Ji, J., PLA-PBAT-PLA tri-block copolymers: Effective compatibilizers for promotion of the mechanical and rheological properties of PLA/PBAT blends. *Polym. Degrad. Stab.* **2018,** *147,* 41-48.

22. Pitet, L. M.; Wuister, S. F.; Peeters, E.; Kramer, E. J.; Hawker, C. J.; Meijer, E. W., Well-Organized Dense Arrays of Nanodomains in Thin Films of Poly(dimethylsiloxane)-b-poly(lactide) Diblock Copolymers. *Macromolecules* **2013,** *46,* 8289-8295.

23. Hirata, M.; Masutani, K.; Kimura, Y., Synthesis of ABCBA Penta Stereoblock Polylactide Copolymers by Two-Step Ring-Opening Polymerization of l- and d-Lactides with Poly(3-methyl-1,5-pentylene succinate) as Macroinitiator (C): Development of Flexible Stereocomplexed Polylactide Materials. *Biomacromol.* **2013,** *14,* 2154-2161.

24. Xiao, R. Z.; Zeng, Z. W.; Zhou, G. L.; Wang, J. J.; Li, F. Z.; Wang, A. M., Recent advances in PEG-PLA block copolymer nanoparticles. *Int J Nanomedicine* **2010,** *5,* 1057-1065.

25. Krajovic, D. M.; Kumler, M. S.; Hillmyer, M. A., PLA Block Polymers: Versatile Materials for a Sustainable Future. *Biomacromol.* **2025,** *26,* 2761-2783.

26. Oh, J. K., Polylactide (PLA)-based amphiphilic block copolymers: synthesis, self-assembly, and biomedical applications. *Soft Matter.* **2011,** *7,* 5096-5108.

27. Li, T.; Zhang, J.; Schneiderman, D. K.; Francis, L. F.; Bates, F. S., Toughening Glassy Poly(lactide) with Block Copolymer Micelles. *ACS Macro Lett.* **2016,** *5,* 359-364.

28. Theryo, G.; Jing, F.; Pitet, L. M.; Hillmyer, M. A., Tough Polylactide Graft Copolymers. *Macromolecules* **2010,** *43,* 7394-7397.

29. Pitet, L. M.; Hillmyer, M. A., Combining Ring-Opening Metathesis Polymerization and Cyclic Ester Ring-Opening Polymerization To Form ABA Triblock Copolymers from 1,5-Cyclooctadiene and d,l-Lactide. *Macromolecules* **2009,** *42,* 3674-3680.

30. Anderson, K.; Schreck, K.; Hillmyer, M., Toughening Polylactide. *Polym. Rev.* **2008,** *48,* 85-108.

31. Kumar, R.; Goswami, M.; Mays, J.; Sumpter, B.; Wang, X., Morphologies of block copolymers composed of charged and neutral blocks. *Soft Matter.* **2012,** *8*.

32. Maji, P.; Naskar, K., Styrenic block copolymer-based thermoplastic elastomers in smart applications: Advances in synthesis, microstructure, and structure–property relationships—A review. *J. Appl. Polym. Sci.* **2022,** *139,* e52942.

33. Lee, S.; Lee, K.; Jang, J.; Choung, J. S.; Choi, W. J.; Kim, G.-J.; Kim, Y.-W.; Shin, J., Sustainable poly(ε-decalactone)−poly(l-lactide) multiarm star copolymer architectures for thermoplastic elastomers with fixed molar mass and block ratio. *Polymer* **2017,** *112,* 306-317.

34. Nomura, K.; Peng, X.; Kim, H.; Jin, K.; Kim, H.; Bratton, A.; Bond, C.; Broman, A.; Miller, K.; Ellison, C., Multiblock Copolymers for Recycling Polyethylene-Poly(ethylene terephthalate) Mixed Waste. *ACS Appl. Mater. Interfaces* **2020,** *12,* 9726-9735.

35. Li, J.; Guo, S.; Wang, M.; Ye, L.; Yao, F., Poly(lactic acid)/poly(ethylene glycol) block copolymer based shell or core cross-linked micelles for controlled release of hydrophobic drug. *RSC Adv.* **2015,** *5,* 19484-19492.

36. Wanamaker, C. L.; Bluemle, M. J.; Pitet, L. M.; O'Leary, L. E.; Tolman, W. B.; Hillmyer, M. A., Consequences of polylactide stereochemistry on the properties of polylactide-polymenthide-polylactide thermoplastic elastomers. *Biomacromol.* **2009,** *10,* 2904-11.

37. Blankenship, J. R.; Levi, A. E.; Goldfeld, D. J.; Self, J. L.; Alizadeh, N.; Chen, D.; Fredrickson, G. H.; Bates, C. M., Asymmetric Miktoarm Star Polymers as Polyester Thermoplastic Elastomers. *Macromolecules* **2022,** *55,* 4929-4936.

38. Liffland, S.; Kumler, M.; Hillmyer, M. A., High Performance Star Block Aliphatic Polyester Thermoplastic Elastomers Using PDLA-b-PLLA Stereoblock Hard Domains. *ACS Macro Lett.* **2023,** *12,* 1331-1338.

39. Albanese, K. R.; Blankenship, J. R.; Quah, T.; Zhang, A.; Delaney, K. T.; Fredrickson, G. H.; Bates, C. M.; Hawker, C. J., Improved Elastic Recovery from ABC Triblock Terpolymers. *ACS Polym Au* **2023,** *3,* 376-382.

40. Fournier, L.; Rivera Mirabal, D. M.; Hillmyer, M. A., Toward Sustainable Elastomers from the Grafting-Through Polymerization of Lactone-Containing Polyester Macromonomers. *Macromolecules* **2022,** *55,* 1003-1014.

41. Sun, S.; Weng, Y.; Zhang, C., Recent advancements in bio-based plasticizers for polylactic acid (PLA): A review. *Polym. Test.* **2024,** *140,* 108603.

42. Wilbon, P. A.; Chu, F.; Tang, C., Progress in Renewable Polymers from Natural Terpenes, Terpenoids, and Rosin. *Macromol. Rapid Commun.* **2013,** *34,* 8-37.

43. Wahlen, C.; Blankenburg, J.; von Tiedemann, P.; Ewald, J.; Sajkiewicz, P.; Müller, A. H. E.; Floudas, G.; Frey, H., Tapered Multiblock Copolymers Based on Farnesene and Styrene: Impact of Biobased Polydiene Architectures on Material Properties. *Macromolecules* **2020,** *53,* 10397-10408.

44. Den Haese, M.; Gemoets, H. P. L.; Van Aken, K.; Pitet, L. M., Fully biobased triblock copolymers generated using an unconventional oscillatory plug flow reactor. *Polym. Chem.* **2022,** *13,* 4406-4415.

45. Yoo, T.; Henning, S., Synthesis and characterization of farnesene-based polymers. *Rubber Chem. Technol.* **2017,** *90,* 308-324.

46. Meier-Merziger, M.; Fickenscher, M.; Hartmann, F.; Kuttich, B.; Kraus, T.; Gallei, M.; Frey, H., Synthesis of phase-separated super-H-shaped triblock architectures: poly(l-lactide) grafted from telechelic polyisoprene. *Polym. Chem.* **2023,** *14,* 2820-2828.

47. Fan, L.; Zhang, L.; Shen, Z., Characteristics and Kinetics of Ring-opening Polymerization of ε-Caprolactone Initiated by Lanthanide Tris(2,4,6-trimethylphenolate)s. *Polym. J.* **2004,** *36,* 91-95.

48. Mazarro, R.; Gracia, I.; Rodríguez, J. F.; Storti, G.; Morbidelli, M., Kinetics of the ring-opening polymerization of D,L-lactide using zinc (II) octoate as catalyst. *Polym. Int.* **2012,** *61,* 265-273.

49. Drayer, W. F.; Simmons, D. S., Is the Molecular Weight Dependence of the Glass Transition Temperature Driven by a Chain End Effect? *Macromolecules* **2024,** *57,* 5589-5597.

50. Zhou, C.; Wei, Z.; Wang, Y.; Yu, Y.; Leng, X.; Li, Y., Fully biobased thermoplastic elastomers: Synthesis of highly branched star comb poly(β-myrcene)-graft-poly(l-lactide) copolymers with tunable mechanical properties. *Eur. Polym. J.* **2018,** *99,* 477-484.

51. Pitet, L. M.; Amendt, M. A.; Hillmyer, M. A., Nanoporous Linear Polyethylene from a Block Polymer Precursor. *J. Am. Chem. Soc.* **2010,** *132,* 8230-8231.

52. Hamley, I. W.; Castelletto, V., Small-angle scattering of block copolymers: in the melt, solution and crystal states. *Prog. Polym. Sci.* **2004,** *29,* 909-948.

53. Tropp, J.; Meli, D.; Wu, R.; Xu, B.; Hunt, S. B.; Azoulay, J. D.; Paulsen, B. D.; Rivnay, J., Revealing the Impact of Molecular Weight on Mixed Conduction in Glycolated Polythiophenes through Electrolyte Choice. *ACS Mater. Lett.* **2023,** *5,* 1367-1375.

54. Lin, Y.-H.; Yager, K. G.; Stewart, B.; Verduzco, R., Lamellar and liquid crystal ordering in solvent-annealed all-conjugated block copolymers. *Soft Matter.* **2014,** *10,* 3817-3825.

55. Li, X.; Li, J.; Wang, C.; Liu, Y.; Deng, H., Fast self-assembly of polystyrene-b-poly(fluoro methacrylate) into sub-5 nm microdomains for nanopatterning applications. *J. Mater. Chem. C* **2019,** *7,* 2535-2540.

56. Tambasco, M.; Lipson, J. E. G.; Higgins, J. S., Blend Miscibility and the Flory−Huggins Interaction Parameter: A Critical Examination. *Macromolecules* **2006,** *39,* 4860-4868.

57. Rabotyagova, O. S.; Cebe, P.; Kaplan, D. L., Protein-based block copolymers. *Biomacromol.* **2011,** *12,* 269-89.

58. Kamata, K.; Iyoda, T., CHAPTER 5 - Nanocylinder Array Structures in Block Copolymer Thin Films. In *Nanomaterials*, Hosono, H.; Mishima, Y.; Takezoe, H.; MacKenzie, K. J. D.; MacKenzie, K.; Mishima, Y.; Takezoe, H., Eds. Elsevier Science Ltd: Oxford, 2006; pp 171-223.

59. Peña-Alcántara, A.; Nikzad, S.; Michalek, L.; Prine, N.; Wang, Y.; Gong, H.; Ponte, E.; Schneider, S.; Wu, Y.; Root, S. E.; He, M.; Tok, J. B. H.; Gu, X.; Bao, Z., Effect of Molecular Weight on the Morphology of a Polymer Semiconductor–Thermoplastic Elastomer Blend. *Adv. Electron. Mater.* **2023,** *9,* 2201055.

60. Matsen, M. W.; Bates, F. S., Conformationally asymmetric block copolymers. *J. Polym. Sci., Part B: Polym. Phys.* **1997,** *35,* 945-952.

61. Koneripalli, N.; Bates, F. S.; Fredrickson, G. H., Fractal Hole Growth in Strained Block Copolymer Films. *Phys. Rev. Lett.* **1998,** *81,* 1861-1864.

62. Kim, J. U.; Matsen, M. W., Repulsion Exerted on a Spherical Particle by a Polymer Brush. *Macromolecules* **2008,** *41,* 246-252.

63. Matsen, M. W., Effect of Architecture on the Phase Behavior of AB-Type Block Copolymer Melts. *Macromolecules* **2012,** *45,* 2161-2165.

64. Milner, S. T., Chain Architecture and Asymmetry in Copolymer Microphases. *Macromolecules* **1994,** *27,* 2333-2335.

65. Minehara, H.; Pitet, L. M.; Kim, S.; Zha, R. H.; Meijer, E. W.; Hawker, C. J., Branched Block Copolymers for Tuning of Morphology and Feature Size in Thin Film Nanolithography. *Macromolecules* **2016,** *49,* 2318-2326.

66. Pitet, L. M.; Chamberlain, B. M.; Hauser, A. W.; Hillmyer, M. A., Dispersity and architecture driven self-assembly and confined crystallization of symmetric branched block copolymers. *Polym. Chem.* **2019,** *10,* 5385-5395.

67. Cheng, B.-X.; Gao, W.-C.; Ren, X.-M.; Ouyang, X.-Y.; Zhao, Y.; Zhao, H.; Wu, W.; Huang, C.-X.; Liu, Y.; Liu, X.-Y.; Li, H.-N.; Li, R. K. Y., A review of microphase separation of polyurethane: Characterization and applications. *Polym. Test.* **2022,** *107,* 107489.

68. Mai, S.-M.; Mingvanish, W.; Turner, S. C.; Chaibundit, C.; Fairclough, J. P. A.; Heatley, F.; Matsen, M. W.; Ryan, A. J.; Booth, C., Microphase-Separation Behavior of Triblock

669 Copolymer Melts. Comparison with Diblock Copolymer Melts. *Macromolecules* **2000,** *33,* 5124-
670 5130.

671 69. Matsen, M. W.; Thompson, R. B., Equilibrium behavior of symmetric ABA triblock
672 copolymer melts. *J. Chem. Phys.* **1999,** *111,* 7139-7146.

673 70. Matsen, M. W.; Schick, M., Stable and unstable phases of a diblock copolymer melt. *Phys.*
674 *Rev. Lett.* **1994,** *72,* 2660-2663.

675 71. Matsen, M. W.; Bates, F. S., Unifying Weak- and Strong-Segregation Block Copolymer
676 Theories. *Macromolecules* **1996,** *29,* 1091-1098.

677 72. Kota, T.; Imaizumi, K.; Sasaki, S.; Sakurai, S., Spontaneous Enhancement of Packing
678 Regularity of Spherical Microdomains in the Body-Centered Cubic Lattice upon Uniaxial
679 Stretching of Elastomeric Triblock Copolymers. *Polymers (Basel)* **2011,** *3,* 36-50.

680 73. Kim, K.; Arora, A.; Lewis, R. M.; Liu, M.; Li, W.; Shi, A.-C.; Dorfman, K. D.; Bates, F.
681 S., Origins of low-symmetry phases in asymmetric diblock copolymer melts. *Proc. Natl. Acad. Sci.*
682 *U.S.A.* **2018,** *115,* 847-854.

683 74. Balsara, N. P., Kinetics of phase transitions in block copolymers. *Curr. Opin. Solid State*
684 *Mater. Sci.* **1999,** *4,* 553-558.

685 75. Kim, H. J.; Jin, K.; Shim, J.; Dean, W.; Hillmyer, M. A.; Ellison, C. J., Sustainable Triblock
686 Copolymers as Tunable and Degradable Pressure Sensitive Adhesives. *ACS Sustain. Chem.*
687 *Eng.* **2020,** *8,* 12036-12044.

688 76. Sheldon, R. A., The E factor at 30: a passion for pollution prevention. *Green Chem.* **2023,**
689 *25,* 1704-1728.

690 77. Chamas, A.; Moon, H.; Zheng, J.; Qiu, Y.; Tabassum, T.; Jang, J. H.; Abu-Omar, M.;
691 Scott, S. L.; Suh, S., Degradation Rates of Plastics in the Environment. *ACS Sustain. Chem. Eng.*
692 **2020,** *8,* 3494-3511.

693 78. Luk, S. B.; Métafiot, A.; Morize, J.; Edeh, E.; Marić, M., Hydrogenation of poly(myrcene)
694 and poly(farnesene) using diimide reduction at ambient pressure. *Journal of Polymer Science*
695 **2021,** *59,* 2140-2153.

696

697

698

699

700

701

For Table of Contents

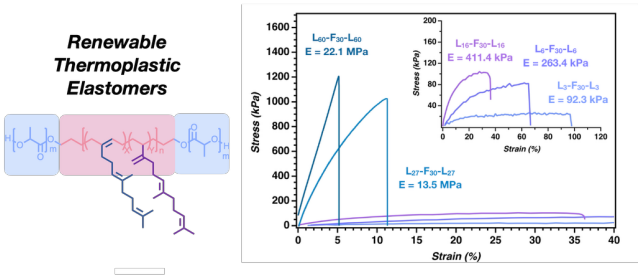

Renewable block polymers have been synthesized in a process with improved sustainability, shown to self-assemble and exhibit elastomeric behavior.